Electronic Raman response of a superconductor across a time reversal symmetry breaking phase transition

Surajit Sarkar [1] and Saurabh Maiti [1,2,*]
[1]*Department of Physics, Concordia University, Montreal, QC H4B 1R6, Canada*
[2]*Centre for Research in Molecular Modelling, Concordia University, Montreal, QC H4B 1R6, Canada*

(Received 15 December 2023; revised 27 February 2024; accepted 29 February 2024; published 20 March 2024)

Polarization-resolved electronic Raman spectroscopy is an important experimental tool to investigate collective excitations in superconductors. In this paper, we present a general theory that allows us to study the evolution of all Raman active collective modes in multiple symmetry channels across a time reversal symmetry (TRS) breaking superconducting transition. This comprehensive approach reveals that multiple modes belonging to different symmetry channels show a tendency to soften, even when the interactions in the subleading channel are held constant. This indicates an increased competition induced by the proximity to the TRS breaking transition. The entry into the TRS broken phase is marked by the introduction of an additional mode into the gap in multiple symmetry channels. This additional modes have a phase character complementary to the ones that are already present. Even though all the modes in the TRS broken phase acquire an amplitude character, we explicitly demonstrate that the coupling to the Raman probe is exclusively through the phase sector. We demonstrate that the Raman spectrum collected in lower symmetry channels shows a selective sensitivity to the sign of the ground-state order parameters and the sign of the interband interactions. Finally, we demonstrate the applicability of an interaction induced selection rule that clearly explains the spectral weights of various modes in various irreducible representations, including the possible of dark Leggett and Bardasis-Schrieffer modes.

DOI: 10.1103/PhysRevB.109.094515

I. INTRODUCTION

The use of electronic Raman scattering (eRS) to study the superconducting phase has a long history dating back to the study of 2*H*-$NbSe_2$ [1], where superconductivity coexists with a charge density wave. The interest in those days focused on understanding the coupling of phonon modes (either from the lattice of ions or from electrons as in a charge density wave) to superconductivity [2–4], as it was assumed that the Cooper pair excitations, which were argued to be small [5], would have a weak strength in the eRS spectra. After it was demonstrated (in A15 compounds) that these excitations could have observable spectra weight without the aid of phonons [6], eRS was used to find the T_c, the size, temperature evolution, and even symmetry of the order parameter [7–9]. Many other uses of eRS to explore quantum phenomena in materials that are associated with superconductivity followed [10]. While phonons and magnons were the early (extrinsic) collective modes of interest to eRS, a purely electronic collective mode that was observed in MgB_2 [11] paved the way for eRS to be used to explore the nature and type of electronic correlations. Indeed, in the context of superconductivity, eRS was subsequently used to affirm the role of spin fluctuations in the pairing mechanism in the Fe-based superconductors [12,13] and identifying higher symmetry charge fluctuations [14].

These developments, along with the fact that the same eRS experiment can provide access to excitations of the system in different irreducible representations (irreps) of the lattice simply by selecting the polarization of incoming and scattered light, encouraged both experimentalists and theorists to explore the role of correlations in the various quantum phases of matter. For example, all features of the eRS spectrum in the A_{1g} irrep for MgB_2, which is a two-band system, were successfully explained by theory [15,16]. However, subsequent theoretical studies for other materials suffered from limitations that prevented one from convincingly interpreting all features of eRS data. These limitations include the fact that most data from multiband systems were fitted using models for one-band systems or systems idealized to have identical gaps and that the models were limited to one specific irrep at a time [17–19]. These were limitations because they never explained the simultaneous presence of significant spectral weight in both the collective mode and the 2Δ threshold of Cooper-pair excitations, which is a common feature in many experiments. One had to invoke the presence of independent bands to explain such features, which is unrealistic in coupled multiband systems. This issue was soon addressed in Ref. [20] that presented a general microscopic formalism to model a multiband eRS response with effects of electronic correlations in any symmetry channel for any pairing symmetry. This theoretical development allowed one to study the properties of any microscopic model with any number of bands based on a Fermi liquid normal state. On this front, one recently demonstrated the existence of additional interaction induced

*saurabh.maiti@concordia.ca

selection rules for the coupling of electronic collective modes [21] to eRS that is applicable in all irreps.

In this paper, we demonstrate another use of the general formalism and the interaction-induced selection rule applied to the eRS response from a time reversal symmetry (TRS) breaking superconductor and discuss the spectrum in various irreps across the phase boundary of a TRS to TRS breaking phase transition. We address questions about the number of collective modes across this transition, their energies, their character (what is the physical quantity that is fluctuating), their spectral weights in eRS, and if there are any characteristic changes between the two phases or across the transition. Our model even allows us to investigate the eRS spectra in different irreps. The motivation behind this type of study stems from the fact that TRS breaking superconductivity has attracted a lot of attention in recent years due to its application in topological quantum computation and other quantum devices [22,23]. Typical means of detecting TRS breaking are through the muon spin relaxation and the polar Kerr effect measurements. Indeed these tools were used to detect TRS breaking in UPt_3 [24,25], Sr_2RuO_4 [26,27], URu_2Si_2 [28], and in K-doped $BaFe_2As_2$ [29–31]. There are more predictions for the TRS breaking state that are awaiting experimental affirmation such as for doped graphene [32] and Moiré heterostructures [33,34]. While detecting TRS breaking was possible, the order parameter is still debated in many of these materials [25,35]. It is therefore beneficial to look for other probes that could provide some details about the order parameter structure while still possibly detecting the TRS breaking transition. In this paper, we provide the initial steps toward modeling the eRS from such systems by studying the $s + is$ state that has been identified in K-doped $BaFe_2As_2$.

The collective modes of a TRS breaking superconductor are partially known and are expected to couple to the eRS spectrum in general. However, the response itself has never been modeled microscopically, presumably because of a lack of theoretical progress. With our model, we can study the behavior of all the collective modes in the amplitude, phase, and density sectors, all the way across a phase boundary, and model their spectral weights in various irreps of the eRS. We show that this can allow us to infer the phase of the order parameter, the attractive or repulsive nature of interactions, and even the phase boundary of the transition. There are many previously unacknowledged results about the collective mode spectrum and its coupling to eRS in such a system which we will spell out in the next section.

The rest of this paper is organized as follows. In Sec. II, we present some historical discussion of the collective modes of a superconductor and their expected spectral weights and then summarize our main results in the context of this historical background. In Sec. III, we summarize the multiband model for eRS in singlet superconductors and provide some general considerations of the nature of collective modes and how they couple to the Raman probe. In Sec. IV, we present a toy three-band model that has a TRS-to-TRS-breaking-phase boundary. In Sec. V A, we apply our general multiband theory across the entire phase diagram and discuss the eRS spectrum in the A_{1g} irrep. In Sec. V B, we discuss the eRS spectrum in the B_{1g} irrep. In Sec. VI, we present our conclusions and some future directions.

II. A BRIEF HISTORY AND MAIN RESULTS

A. Collective modes and their spectral weights

The collective modes in a superconductor correspond to coherent fluctuations of the order parameter (also referred to as the excitations of the Cooper pair). In a single-band superconductor (we only focus on clean systems at $T = 0$), there are two collective modes. One corresponds to the coherent fluctuations of the order parameter strength (amplitude): the massive Anderson-Higgs (AH) mode [36,37]. This mode does not directly couple to spectroscopic probes in the linear regime (unless mediated by phonons [2–4,38] or external supercurrent [39]). The other mode corresponds to the coherent fluctuations of the phase of the order parameter: the massless Bogoliubov-Anderson-Goldstone (BAG) mode [36,40,41]. Modes in the phase sector couple to density fluctuations which in turn directly couple to photons. The BAG mode, although expected due to the spontaneous breaking of U(1) symmetry, is renormalized by the Coulomb interaction to the plasma frequency and hence not accessible at low energies [42]. Even if they were probed at higher energies, the spectral weight associated with this mode would be $\propto q^2 \to 0$ [37,43], where q is the momentum transferred by photons, rendering it undetectable. If there were competing Cooper channel interactions in irreps other than the ground state one, then one could expect additional massive collective modes both in phase and amplitude sectors. These phase sector collective modes, which couple to density fluctuations and hence to photons, are called the Bardasis-Schrieffer (BaSh) modes [17,37,44]. While the AH and BAG modes are present but never visible in superconductors, the BaSh mode, when present, is expected to be visible. The presence of the BaSh mode signals a strong competition from a subleading irrep in the Cooper channel.

In a two-band superconductor, the collective excitations include additional massive collective modes. In the phase sector, these are called the Leggett modes [45]. They correspond to the out-of-phase (relative) fluctuations of the order parameters in two bands, as opposed to the in-phase BAG mode which remains massless. Similarly, more modes are expected in higher irreps if there is competition. None of the modes except the BAG are normalized by the Coulomb interaction due to either a symmetry decoupling (from belonging to different angular momentum channels) or due to the fact that the long-range Coulomb interaction is blind to the intra-unit-cell part of the fluctuations that exist in the multiband case [46]. All these additional modes in the phase sector are expected to have finite spectral weight, while the amplitude sector remains inaccessible.

In TRS broken superconductors, however, the amplitude and the phase sector fluctuations are coupled. For a TRS breaking $s + is$ state, the expected collective mode spectrum across this phase transition is such that a Leggett mode softens and bounces back [47–49]. For an $s + id$ transition, there is a mixed-symmetry BaSh mode that is expected to soften and bounce back [50]. There are also other predictions for the existence of collective modes in the TRS broken phases [51–53]. However, their existence does not guarantee their coupling to a probe. Addressing this was one of the main motivations for this paper. Specifically, there are open questions as to if the modes in the phase sector are always expected

to couple to eRS, if the modes in the TRS broken state that include amplitude fluctuations enable an equilibrium coupling of photons to the amplitude sector, and what are the spectral weights of various modes in both states as well as across the transition.

B. Summary of main findings

We worked with the s-to-$(s+is)$ transition that requires at least three bands microscopically. This allows us to use constant gaps which keeps the calculations analytically tractable. The general results for the collective modes are as follows.: (i) In the A_{1g} irrep, there is the expected Leggett mode that softens when approaching the phase boundary from the TRS phase, and it bounces back in the TRS broken phase. Surprisingly, there is a similar tendency in the B_{1g} irrep with the BaSh mode, which happens without altering the B_{1g} interactions. This suggests that the approach to the TRS breaking boundary is marked by competition between $s+is$ and $s+id$ states. (ii) In the TRS broken phase, there is an additional collective mode that is induced near the pair-breaking threshold in both irreps. Both the bounced-back mode and the additional mode have mixed amplitude and phase character of the fluctuations. However, near the TRS breaking transition one of the modes has predominantly an amplitude character, while the other has a phase character. The phase part of the fluctuations of these two modes have complementary characters: if one is in-phase, the other is out-of-phase. (iii) In the B_{1g} sector, we show that, depending on the sign of the interband interactions, either the in-phase or out-of-phase mode could be the low-energy mode. This is helpful, as it indicates the phase characteristic of the competing d-wave state in terms of it being of the d^{++} or d^{+-} type.

The general results for the manifestation of collective modes in eRS are far more interesting, which can be explicitly inferred from the formulas we derive but, in many cases, can also be deduced from the interaction-induced selectivity of modes outlined in Ref. [21] (cf. Secs. V A and V B below). These findings are as follows: (i) Despite the mixing of the phase and amplitude fluctuations, the coupling to eRS comes exclusively from the phase fluctuations of the collective mode. This is true in all irreps. (ii) In both the TRS and TRS broken phases, the A_{1g} response is not sensitive to the sign of the gaps in the ground state, but the B_{1g} response is, and this could serve as means to detect sign changes of the order parameter. (iii) There is a possibility of a dark Leggett mode and a BaSh mode that prevents these modes from coupling to eRS. Thus, a phase transition could be triggered without a visible softening of a mode. (iv) The spectral weight near the pair-breaking continuum does not display any characteristic change across the transition (except for the introduction of an additional mode into the gap). However, they are characteristically different deep inside and deep outside the TRS broken phase.

The knowledge of the evolution of the character and spectral weight of the modes in different irreps provides a clear picture of the low-energy sector near a TRS breaking transition and could be used to even detect such transitions. In the remainder of this paper, we will substantiate the above statements with detailed explanations and discussions.

III. THE RAMAN RESPONSE IN A MULTIBAND SUPERCONDUCTOR

Consider a multiband system $\mathcal{H} = \mathcal{H}_{\rm MF} + \mathcal{H}_{\rm residual}$. Here, $\mathcal{H}_{\rm MF}$ is the mean-field part of the Hamiltonian in the singlet channel given by

$$\mathcal{H}_{\rm MF} = \sum_{\alpha,\vec{k}} \Psi^\dagger_\alpha(\vec{k})\hat{\mathcal{E}}_\alpha(\vec{k})\Psi_\alpha(\vec{k}),$$

where $\hat{\mathcal{E}}_\alpha(\vec{k}) = \varepsilon_{\alpha,\vec{k}}\hat{\sigma}_3 - \Delta^R_{\alpha,\vec{k}}\hat{\sigma}_1 + \Delta^I_{\alpha,\vec{k}}\hat{\sigma}_2$, and $\Psi_\alpha(\vec{k}) = (\hat{c}_{\alpha,\vec{k},\uparrow}\ \hat{c}^\dagger_{\alpha,-\vec{k},\downarrow})$. The index $\alpha \in \{a, b, \dots\}$ represents the bands, $\hat{\sigma}_0$ is a 2×2 identity matrix, and $\hat{\sigma}_i, i \in \{1,2,3\}$ are the Pauli matrices in the particle-hole space. Further, $\varepsilon_{\alpha,\vec{k}}$ is the dispersion of αth band, and $\hat{c}_{\alpha\vec{k}s}$ denotes the annihilation operator for the quantum state in band α, momentum $\vec{k}$, and spin s. Finally, $\Delta_{\alpha,\vec{k}} \equiv \Delta^R_{\alpha,\vec{k}} + i\Delta^I_{\alpha,\vec{k}}$ is the mean-field order parameter. Here, $\mathcal{H}_{\rm residual}$ denotes the residual interactions in the Cooper channel that correspond to momentum transfers $\vec{q} \neq 0$, where $\vec{q} = 0$ is the momentum transfer channel in which the condensation took place [20,54]. These interactions include density-density interaction within the same band as well as density-density, exchange, and pair-hopping interactions between fermions from different bands. Of these interactions, however, what is relevant for the superconductivity problem is just the Cooper channel projection of the interactions (see Ref. [20]), which we model as $V^{\rm pp}_{\alpha\beta}$ between two bands α and β. In what follows, to ensure analytical tractability, we shall work at temperature $T = 0$ with $\vec{k}$-independent interactions, which results in $\vec{k}$-independent order parameters $\Delta_\alpha = \Delta^R_\alpha + i\Delta^I_\alpha$, which satisfy the self-consistency equations:

$$\Delta_\alpha = -\sum_\beta V^{\rm pp}_{\alpha\beta}\Delta_\beta \nu^\beta_F l_\beta, \tag{1}$$

where ν^β_F is the density of states at the Fermi level of band β, and $l_\beta \equiv \ln(2\Lambda/|\Delta_\beta|)$, where Λ is some cutoff associated with the pairing mechanism.

It was shown in Ref. [20] that, for $\vec{q} \to 0$ (the momentum transferred by light to the superconductor), the long-range Coulomb interaction did not affect the response. This allows us to unify the treatment of the Raman response in all irreps r of the lattice, which is computed as $\mathrm{Im}[\chi_r(\Omega)]$, where $\chi_r(\Omega)$ is obtained from the analytic continuation of [20]:

$$\chi_r(Q) = -[c_r]^T[[\Pi]][\Gamma_r], \tag{2}$$

where

$$\begin{aligned}
[c_r] &= \left(0, 0, \gamma^a_r, 0, 0, \gamma^b_r, \dots\right)^T,\\
[[\Pi]] &= \mathrm{Diag}([\Pi^a], [\Pi^b], \dots),\\
[\Pi^\alpha] &= \Pi^\alpha_{ij}(Q), \quad \text{for } i,j \in \{1,2,3\},\\
\Pi^\alpha_{ij}(Q) &\equiv \int_K \mathrm{Tr}[\hat{\sigma}_i\hat{\mathcal{G}}_\alpha(K)\hat{\sigma}_j\hat{\mathcal{G}}_\alpha(K+Q)],\\
[\Gamma_r] &= [\mathcal{R}]^{-1}[c_r],\\
[\mathcal{R}] &= \mathbb{I}_{3n\times 3n} + \frac{1}{2}\left[\left[V^{\rm pp}_r\right]\right][[\Pi^{\rm pp}]],\\
[[V^{\rm pp}_r]] &= V^{\rm pp}_{r,\alpha\beta} \otimes \mathbb{I}_{3\times 3},
\end{aligned}$$

$$[[\Pi^{\rm pp}]] = {\rm Diag}([\Pi^{\rm pp,a}], [\Pi^{\rm pp,b}], \dots),$$
$$[\Pi^{{\rm pp},\alpha}] = -\begin{pmatrix} \Pi^{\alpha}_{11} & \Pi^{\alpha}_{12} & \Pi^{\alpha}_{13} \\ \Pi^{\alpha}_{21} & \Pi^{\alpha}_{22} & \Pi^{\alpha}_{23} \\ 0 & 0 & 0 \end{pmatrix},$$

where γ_r^α is the projection of the effective mass vertex of band α onto the rth irrep, n is the number of bands, $K \equiv (i\omega_n, \vec{k})$, $Q \equiv (i\Omega_m, \vec{q})$, $\int_K \equiv T\sum_n \int d^dk/(2\pi)^d$ (where d is the spatial dimension), and $\mathcal{G}_\alpha(i\omega_n, \vec{k})$ is the Green's function:

$$\hat{\mathcal{G}}_\alpha(i\omega_n, \vec{k}) = [i\omega_n\hat{\sigma}_0 - \hat{\mathcal{E}}_\alpha(\vec{k})]^{-1}. \tag{3}$$

Further, $V^{\rm pp}_{r,\alpha\beta}$ is the projection of the Cooper channel interaction onto the rth irrep. In the above expression for the Raman response, we have ignored the contributions from interactions in the particle-hole channel. See Ref. [20] for its inclusion. Continuing on to real frequencies with $i\Omega_m \to \Omega + i\delta$, the various correlation functions Π^α_{ij} are evaluated as

$$\begin{aligned}
\frac{\Pi^\alpha_{11}(\Omega)}{2\nu_F^\alpha} &= -l_\alpha - \left[\left(\frac{\Omega}{2|\Delta_\alpha|}\right)^2 - \left(\frac{\Delta^R_\alpha}{|\Delta_\alpha|}\right)^2\right]\mathcal{I}_\alpha(\Omega), \\
\frac{\Pi^\alpha_{22}(\Omega)}{2\nu_F^\alpha} &= -l_\alpha - \left[\left(\frac{\Omega}{2|\Delta_\alpha|}\right)^2 - \left(\frac{\Delta^I_\alpha}{|\Delta_\alpha|}\right)^2\right]\mathcal{I}_\alpha(\Omega), \\
\frac{\Pi^\alpha_{33}(\Omega)}{2\nu_F^\alpha} &= -\mathcal{I}_\alpha(\Omega), \\
\frac{\Pi^\alpha_{12}(\Omega)}{2\nu_F^\alpha} &= -\left(\frac{\Delta^R_\alpha\Delta^I_\alpha}{|\Delta_\alpha|^2}\right)\mathcal{I}_\alpha(\Omega) = \frac{\Pi^\alpha_{21}(\Omega)}{2\nu_F^\alpha}, \\
\frac{\Pi^\alpha_{13}(\Omega)}{2\nu_F^\alpha} &= -i\left(\frac{\Omega\Delta^I_\alpha}{2|\Delta_\alpha|^2}\right)\mathcal{I}_\alpha(\Omega) = -\frac{\Pi^\alpha_{31}(\Omega)}{2\nu_F^\alpha}, \\
\frac{\Pi^\alpha_{23}(\Omega)}{2\nu_F^\alpha} &= -i\left(\frac{\Omega\Delta^R_\alpha}{2|\Delta_\alpha|^2}\right)\mathcal{I}_\alpha(\Omega) = -\frac{\Pi^\alpha_{32}(\Omega)}{2\nu_F^\alpha},
\end{aligned} \tag{4}$$

where

$$\mathcal{I}_\alpha(\Omega) = \frac{\sin^{-1}(\Omega/2|\Delta_\alpha|)}{(\Omega/2|\Delta_\alpha|)\sqrt{1-(\Omega/2|\Delta_\alpha|)^2}}.$$

In all of the above expressions Ω is to be seen as $\Omega + i\delta$. In Π^α_{ij}, $i = 1$ is associated with the amplitude-sector fluctuations, $i = 2$ is associated with the phase-sector fluctuations, and $i = 3$ is the density-sector fluctuations. Technically, $[\Pi^{\rm pp}]$ is not given in terms of Π^α_{ij} but a quantity whose integrand is the same as Π^α_{ij} but dressed with normalized angular form factors of the rth irrep. Since our Δ_α's are all $\vec{k}$ independent, the angular integration always yields unity, leading to the above form of the equations. We include Δ^I_α in this formalism compared with the previous works [20]. For the sake of completeness, we remind the reader that, in Eq. (2), the vector structure of $[c_r]$ is partitioned into groups of three for each band, with the first two components corresponding to the amplitude and phase degrees of freedom and the third to the density degree of freedom (and hence the only nonzero component). Similarly, in the particle-particle channel, $[\Pi^{{\rm pp},\alpha}]$ couples only to the Cooper-channel interactions and hence has only two rows. The third row would correspond to the particle-hole channel (see $[\Pi^{{\rm ph},\alpha}]$ in Eq. (6)).

A. General considerations

The resonances in the Raman response are captured as poles of $[\Gamma_r]$ which stem from the zeros of Det$[\mathcal{R}]$, where $\mathcal{R}$ is a $3n \times 3n$ matrix for the case of n bands. The 3 arises from the amplitude, phase, and density degrees of freedom in the superconductor. We can estimate the number of zeros in the following manner. Focus first on the region $\Omega \ll 2|\Delta|$, where the frequency dependence is such that Π^α_{11} and $\Pi^\alpha_{22} \sim \Omega^2$ each, Π^α_{33}, Π^α_{12} are independent of Ω, and Π^α_{13}, Π^α_{23} are linear in Ω [see Eq. (4)] but appear as a product of themselves. Thus, Det$[\mathcal{R}] = 0$ is at best second-order polynomial in Ω^2 per band or $2n$th-degree polynomial overall. It is not of degree $3n$, as Π^α_{33} has no Ω^2 term. Next, due to the global U(1) symmetry, the order parameter at the mean-field level is usually chosen to be real if TRS is preserved, implying $\Delta^I_\alpha = 0$, which leads to $\Pi^\alpha_{12} = 0 = \Pi^\alpha_{13}$ decoupling the amplitude sector from the phase and density sector. This decouples the determinant into products of two nth-order polynomials in Ω^2. This factorization separates the amplitude ($i = 1$) and the phase ($i = 2$) sector modes such that there are n of each. Only the phase sector modes are Raman active (i.e., have finite spectral weight), as this is the sector that couples, via nonzero Π^α_{23}, to the effective mass vertex that involves the density vertex with $i = 3$, which in turn couples to photons. Observe also that, if we had chosen the gap to be purely imaginary, then $\Delta^R_\alpha = 0$, leading to $\Pi^\alpha_{23} = 0 = \Pi^\alpha_{21}$. Then Δ^I becomes the amplitude sector and is still decoupled from the phase ($i = 1$) and density ($i = 3$) sectors.

If we did not assume anything about the ground-state phase, all the components above would be formally coupled. However, note that the coupling of the two sectors via $\Pi^\alpha_{12}, \Pi^\alpha_{13}$ terms do not add any additional powers of Ω^2, leading to the same total mode count of $2n$. Further, the self-consistency equations [which include the U(1) symmetry] will cause any observable result to be only dependent on $|\Delta_\alpha|$, as can be explicitly checked by using Eq. (4) in Eq. (2). This means that the modes would still decouple into n phase-sector modes and n amplitude-sector modes, with only the phase-sector modes being potentially Raman active. This check ensures the U(1) gauge invariance of our formalism. If the ground state breaks TRS, then the result would depend on the complex phase of the order parameter, but this does not affect the mode count, as we already saw above that the inclusion of all the terms of Π^α_{ij} do not add any additional powers of Ω^2. What is different in this case is that the modes would have mixed amplitude and phase character, as was noted in previous works [47–49].

B. The character of the modes

To understand the nature of the modes that are Raman active, let us note a very special property of $\chi^\alpha_{22} \equiv \Pi^\alpha_{22} + 2v_F l_\alpha$, Π^α_{23}, Π^α_{32}, and Π^α_{33}: $\chi^\alpha_{22}\Pi^\alpha_{33} - \Pi_{32}\Pi_{23} = 0$. This can be seen as Det$[\Pi^\alpha_{ij}] = 0$, with $\Pi^\alpha_{22} \to \chi^\alpha_{22}$, where $i, j \in \{2, 3\}$. This property of the zero determinant is responsible for the fact that one of the phase sector collective modes in the channel $r = A_{1g}$ is always the massless BAG mode. This mode is removed from the low-energy sector by the Coulomb interaction but would not have shown up anyway due to its zero

mass. Thus, only $n-1$ modes in the phase sector are Raman active for $r = A_{1g}$, which are the Leggett-type modes. In other irreps, we still have n phase modes that are Raman active, and these are the BaSh-type modes. Note that only modes with $\Omega < 2|\Delta_{\min}|$ (the minimum gap in the system) will be long lived. The modes in the continuum of the pair-breaking excitations will be damped.

It is worth noting (see Appendix A) that, even if we included $\Delta^I_\alpha \neq 0$, we would have $\mathrm{Det}[\Pi^\alpha_{ij}] = 0$, with $i, j \in \{1, 2, 3\}$ and $\Pi^\alpha_{11} \to \chi^\alpha_{11}$, $\Pi^\alpha_{22} \to \chi^\alpha_{22}$ (the correlation functions without the l_α part), ensuring that we still have the BAG in the $r = A_{1g}$ channel. This aspect does not depend on whether TRS is preserved or broken, and hence, the BAG mode is always present and is massless (and is always removed by the Coulomb interaction). What changes in the TRS broken phase is that now all the $2n-1$ modes become Raman active due to the mixing of the amplitude and phase contributions. What can also happen is that some modes from the continuum could be pushed into the gap, leading to better visibility of a mode, but this does not change the mode count.

To quantify the admixing of the amplitude and phase fluctuations for the various modes, we can follow the treatment in Refs. [48,50], where the dynamical form of the self-consistency equation is expanded to linear order in the fluctuating components: $\delta\Delta_\alpha \equiv \delta^R_\alpha + i\delta^I_\alpha$. The presence of nontrivial solutions to this equation for a given value of frequency would indicate that the system supports spontaneous fluctuations at that frequency. This maps the problem of finding collective modes to that of finding the eigenvalues and eigenvectors of the dynamical self-consistency equation of the fluctuating components. The eigenvalues give the collective mode frequencies while the eigenvectors give the character, i.e., the extent of admixture of phase and amplitude fluctuations, of the collective modes.

At a finite wave vector q of the fluctuations, we would also need to account for variation in the density ($\delta\rho_\alpha$), and the general eigenvalue problem would be given by

$$\begin{aligned} 2\delta^R_\alpha &= \sum_\beta V^{\mathrm{pp}}_{\alpha\beta}\big[\Pi^\beta_{11}\delta^R_\beta - \Pi^\beta_{12}\delta^I_\beta + \Pi^\beta_{13}\delta\rho_\beta\big], \\ -2\delta^I_\alpha &= \sum_\beta V^{\mathrm{pp}}_{\alpha\beta}\big[\Pi^\beta_{21}\delta^R_\beta - \Pi^\beta_{22}\delta^I_\beta + \Pi^\beta_{23}\delta\rho_\beta\big], \\ \delta\rho_\alpha &= \sum_\beta V_q\big[\Pi^\beta_{31}\delta^R_\beta - \Pi^\beta_{32}\delta^I_\beta + \Pi^\beta_{33}\delta\rho_\beta\big], \end{aligned} \tag{5}$$

where V_q is the singular Coulomb interaction [$\sim 1/q$ in two dimensions (2D) and $\sim 1/q^2$ in three dimensions (3D)] and is the same for all bands. This can be recast into the form $[\mathcal{K}][\delta] = 0$, where $[\delta] \equiv (\delta^R_a, -\delta^I_b, \delta\rho_a, \delta^R_b, -\delta^I_b, \delta\rho_b, \dots)^T$, and

$$[\mathcal{K}] = \mathbb{I}_{3n\times 3n} + \tfrac{1}{2}\big[\big[V^{\mathrm{pp}}_{gs}\big]\big][[\Pi^{\mathrm{pp}}]] + \tfrac{1}{2}[[V_C]][[\Pi^{\mathrm{ph}}]], \tag{6}$$

where

$$[[V_C]] = 2V_q \begin{pmatrix} 1 & 1 & \cdots & 1 \\ 1 & 1 & \cdots & 1 \\ \vdots & \vdots & \ddots & \vdots \\ 1 & 1 & \cdots & 1 \end{pmatrix}_{n\times n} \otimes \mathbb{I}_{3\times 3},$$

$$[[\Pi^{\mathrm{ph}}]] = \mathrm{Diag}([\Pi^{\mathrm{ph,a}}], [\Pi^{\mathrm{ph,b}}], \dots),$$

$$[\Pi^{\mathrm{ph},\alpha}] = \begin{pmatrix} 0 & 0 & 0 \\ 0 & 0 & 0 \\ \Pi^\alpha_{31} & \Pi^\alpha_{32} & \Pi^\alpha_{33} \end{pmatrix}.$$

Here, V^{pp}_{gs} denotes the pairing interaction in the ground state irrep, as in Eq. (2). The $\mathcal{K}$ is the same matrix $\mathcal{R}$ that appears in the Raman response with $r = gs$. In the specific form in Eq. (2), we dropped the $[V^{\mathrm{ph}}]$ part (see Ref. [20] for the full form) on grounds of studying the effect of only the Cooper channel interactions. In the above eigenvalue problem, the Coulomb interaction only becomes relevant at finite q. Since our focus is on the $q = 0$ part, we will continue to ignore the coupling to the density sector to maintain consistency in our treatment (formally, we are ignoring $1/V_C$ compared with $[[V^{\mathrm{pp}}_{gs}]^{-1}]_{\alpha\beta}$).

Having shown that the linear response matrix ($\mathcal{K}$) and the kernel of the Raman response ($\mathcal{R}$) are the same, the character of the collective modes, which are the zeros of the determinant of $\mathcal{R}$ or $\mathcal{K}$, can now be inferred by studying the corresponding eigenvector whose components represent the weights of the fluctuating terms of Δ_α. To categorize these fluctuations in terms of amplitude and phase, note that

$$\delta\Delta_\alpha \equiv \delta(|\Delta_\alpha|e^{i\phi_\alpha}) \approx e^{i\phi_\alpha}\delta|\Delta_\alpha| + i\Delta_\alpha\delta\phi_\alpha + \dots,$$

where the … stand for higher-order terms in $\delta|\Delta_\alpha|$ and $\delta\phi_\alpha$. Taking the real and imaginary parts of this, we get the expressions for δ^R_α and δ^I_α, which we also get from the eigenvectors of $[\mathcal{K}]$. Inverting this relation, we arrive at the amplitude and phase parts:

$$\begin{aligned} \delta|\Delta_\alpha| &= \delta^R_\alpha\cos\phi_\alpha + \delta^I_\alpha\sin\phi_\alpha, \\ |\Delta_\alpha|\delta\phi_\alpha &= \delta^I_\alpha\cos\phi_\alpha - \delta^R_\alpha\sin\phi_\alpha. \end{aligned} \tag{7}$$

We then define the amplitude and phase characters of a mode m as

$$C^A_m \equiv \sum_\alpha \left|\frac{\delta|\Delta_{\alpha,m}|}{|\Delta_\alpha|}\right|^2, \quad C^P_m \equiv \sum_\alpha |\delta\phi_{\alpha,m}|^2, \tag{8}$$

which simply sums up the weights in the amplitude or phase sector from all the bands.

We will now apply this general formalism of finding collective modes and their character to the minimal model that demonstrates TRS breaking with k-independent interactions.

IV. PHASE DIAGRAM OF THREE-BAND MODEL WITH BROKEN TRS

Consider a system with bands a, b, c. To keep the solution analytically tractable, we make bands b and c identical. This allows us to model the interband interactions in the Cooper channel as

$$V^{\mathrm{pp}}_{\alpha\beta} \to \begin{pmatrix} 0 & V_0 & V_0 \\ V_0 & 0 & V_1 \\ V_0 & V_1 & 0 \end{pmatrix}. \tag{9}$$

Here, we have ignored intraband interactions, as we are mostly interested in the new aspects due to the multiband nature of the pairing problem. Certainly, the formalism can be applied to any general interaction matrix at the cost of studying the effects of more parameters. The most general TRS

broken state in the above model could then be parameterized as $\Delta_a = \Delta_0 > 0$, $\Delta_b = \Delta_1 e^{i\phi}$, and $\Delta_c = \Delta_1 e^{-i\phi}$ ($\Delta_1 > 0$) with the order parameters in bands b and c differing only in phase [55]. Further, the overall scale of the order parameters will be controlled by the cutoff, and hence, a relevant parameter would be $r \equiv \Delta_0/\Delta_1$. In the self-consistency equations, we have the Cooper logarithm l_α, which takes the form $l_a = \ln(2\Lambda/\Delta_0) \equiv l_0$ and $l_b = l_c = \ln(2\Lambda/\Delta_1) \equiv l_1$. Observe that $l_0 = l_1 - \ln r$. Using these in Eq. (1), we get

$$\begin{aligned} r &= -2V_0 \nu_F^1 l_1 \cos\phi, \\ \left(1 + V_1 \nu_F^1 l_1\right)\cos\phi &= -rV_0 \nu_F^0 (l_1 - \ln r), \\ \Delta_1 \sin\phi &= \Delta_1 V_1 \nu_F^1 l_1 \sin\phi, \end{aligned} \tag{10}$$

where ν_F^0, ν_F^1 are the densities of states in band a and bands b, c, respectively. These three equations determine the parameters $r \in [0, \infty)$, $l_1 > 0$, and $\phi \in [0, \pi]$ subject to the condition that $|\cos\phi| < 1$. The parameter l_1 is only sensitive to the overall scale of the gap and is not so interesting to the present discussion.

A. TRS phase

In this phase, $\phi = 0$ or π, and hence, the last line in Eq. (10) is not enforced. The parameter r is obtained by solving the transcendental equation:

$$\left(\frac{\nu_F^0}{\nu_F^1}\right) r^2 + \left(2\nu_F^0 V_0 \ln r + \frac{V_1}{V_0}\right) rc - 2 = 0, \tag{11}$$

where $c = \cos\phi = \pm 1$. Then $\nu_F^1 l_1 = -rc/2V_0$. Since $l_1 > 0$, we have $c = -\mathrm{sgn}(V_0)$. That is, the relative sign between Δ_0 and Δ_1 (s^{++} vs $s^{\pm}$) can be switched with the attractive or repulsive nature of the interband interaction V_0.

To explore the parameter space, consider the limit $V_0 \to 0$, where we get $r = 0$, implying $\Delta_0 = 0$, $\nu_F^1 l_1 = -1/V_1$, and $\phi = 0$ or π. This requires $V_1 < 0$ and is the result of an effective one-band model, where b, c are seen as one with intraband interaction V_1. On the other hand, in the limit $V_1 \to 0$, we still have $\phi = 0$ or π, and have to solve Eq. (11) to find r. In these two limits, we never get a solution where $\phi \neq \{0, \pi\}$, suggesting that, to break TRS, we need both V_0 and V_1 components, thereby enforcing the necessity of three bands for having a TRS broken state. As we change the parameters V_0 and V_1, this TRS phase continues all the way until $\nu_F^1 l_1 = 1/V_1$. This is when the last line in Eq. (10) begins to be valid even for $\phi \neq 0$. This marks the onset of the TRS broken state.

B. TRS broken phase

In this phase, $\nu_F^1 l_1 = 1/V_1 > 0$ is fixed, and then we have

$$\begin{aligned} \cos\phi &= -\frac{V_1}{2V_0} r, \\ r &= \exp\left(\frac{1}{\nu_F^1 V_1} - \frac{V_1}{\nu_F^0 V_0^2}\right), \end{aligned} \tag{12}$$

subject to the condition that $|\cos\phi| < 1$. A cross-section of the phase diagram across the TRS breaking transition is shown in Fig. 1, which is obtained by keeping V_1 fixed and varying V_0. The distinction between ν_F^1 and ν_F^0 only introduces quantitative differences, and thus, for simplicity, we set $\nu_F^1 = \nu_F^0 = \nu_F$ for all computations in this paper. We will be interested in learning what the Raman response looks like across this phase transition.

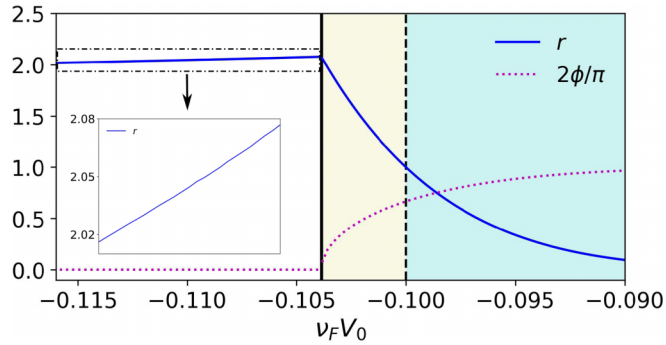

FIG. 1. The parameter $r = \Delta_0/\Delta_1$ with respect to $\nu_F V_0$ across an $s^{++} \to s + is$ transition, which happens at $\nu_F V_0 \approx -0.104$ (indicated by the solid vertical line). Here, the phase ϕ (dotted curve) becomes nontrivial. The vertical dashed line shows the point where $r = 1$ beyond which we label the state as being deep in the TRS broken phase. The phase diagram for $s^{+-} \to s + is$ transition remains the same but with $V_0 \to -V_0$. Here, $\nu_F V_1 = 0.1$ and $\Lambda = 1.5 \times 10^4 \Delta_1$. The inset is provided to highlight the variation in r with $\nu_F V_0$.

V. RESULTS FOR RAMAN RESPONSE

Now that we have a model which provides a phase space of ground states, we can study the eRS response from this model. As outlined earlier, with $n = 3$, we expect a total of $2n - 1 = 5$ collective modes in our system. In the TRS side of the phase diagram, $n - 1 = 2$ of them would be in the phase sector and hence visible in Raman spectroscopy. To figure out the spectral weights and characters of these modes, we can deploy the general result from Sec. III. In Fig. 2, we plot the A_{1g} and B_{1g} responses across the TRS breaking phase transition. The A_{1g} spectrum of collective modes is fixed as soon the ground state is picked because it involves the same interactions and cannot change unless the ground state is changed. The spectral weights, however, will depend on the Raman vertices. Figure 2 is shown for the choice $\gamma_r^b = -\gamma_r^c = 0.5\gamma_r^a$ for $r \in \{A_{1g}, B_{1g}\}$. The result is not surprising: A collective mode (labeled 1) softens at the TRS breaking transition. This mode bounces back and crosses another mode (labeled 2) that is induced in the TRS broken phase from the 2Δ threshold. We plot the character of these modes in Fig. 3, which shows that mode 1 is a pure phase one on the TRS side. It acquires an amplitude character as soon as it enters the TRS broken side, and this character dominates deep inside the TRS broken state. Meanwhile, mode 2 emerges with largely an amplitude character and becomes phase dominant deep inside the TRS broken phase. This mode will go on to soften with increasing V_0, leading to another transition boundary between the $s + is$ state and a different s^{+-} state which has opposite phase of gaps between bands b, c. We do not show that transition here. There is more depth to these results, which will be the subject of the discussion in following subsections.

The B_{1g} collective modes, on the other hand, depend on the choice of interactions in the B_{1g} channel, which are

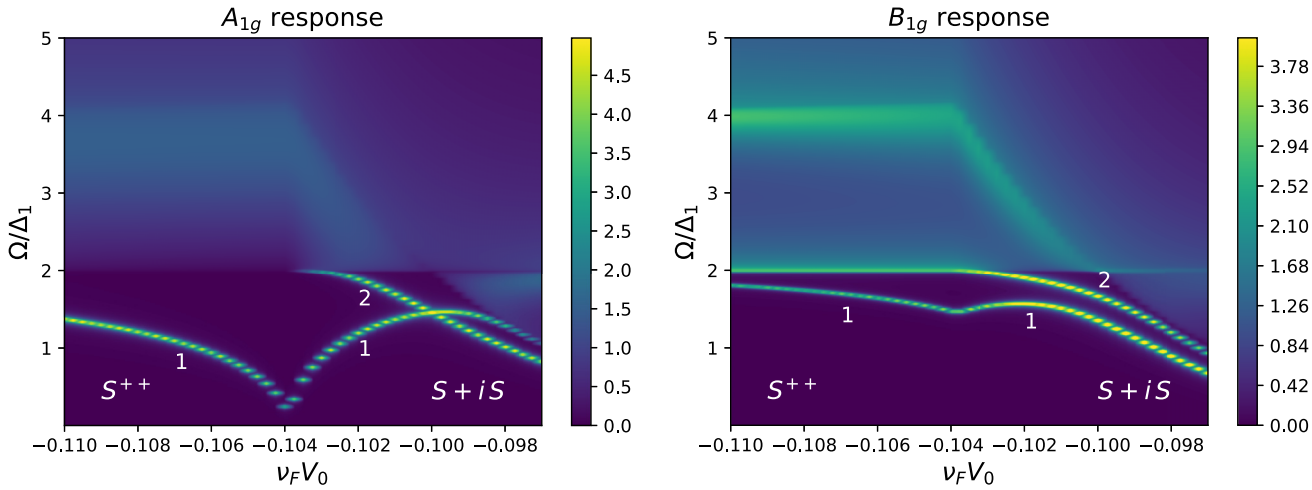

FIG. 2. The eRS response in the A_{1g} and B_{1g} irreps. The A_{1g} mode 1 softens at the $s^{++} \to s + is$ transition ($\nu_F V_0 \approx -0.104$), while the B_{1g} mode 1 turns back. In both cases, an additional mode 2 is induced from the 2Δ threshold inside the TRS broken phase. The choice of Raman vertices in both cases is $\gamma_r^b = -\gamma_r^c$, $r \in \{A_{1g}, B_{1g}\}$. For A_{1g}, all parameters are the same as in Fig. 1. For B_{1g}, the interband interaction elements are $\nu_F U_0 = 0.07$, $\nu_F U_1 = 0$. A fermion lifetime of $0.005\Delta_1$ was added to induce broadening. The color scale corresponds to $\ln(1 + \mathrm{Im}\chi_r/\chi_0)$, where $\chi_0 \propto \nu_F(\gamma_r^a)^2$ is an arbitrary scale to remove the dimensions. This form was chosen to enhance the visibility of the 2Δ region.

independent of the ground state. Figure 2 also shows the B_{1g} response for an interband driven scenario where all three bands are coupled (more details in Sec. V B). It shows a BaSh mode on the TRS side that also has a tendency to soften and bounce back in the TRS broken side. Just like the A_{1g} response, there is another mode that is induced in the TRS broken phase near the 2Δ threshold. What is striking here is that the BaSh mode displays a tendency to soften even though the B_{1g} interactions are held constant. This suggests that the approach toward the TRS breaking state boosts both the competing suborders in the A_{1g} and B_{1g} channels. In fact, if the B_{1g} interaction in the TRS phase is strong enough, the approach toward the TRS breaking state can cause the BaSh mode to soften before the Leggett mode, leading to an $s + id$ state. The type of $s + id$ ground state that would develop (i.e., the relative phase between various bands) depends on the phase character of the mode that softens. As we will discuss shortly, this phase character could be deduced from

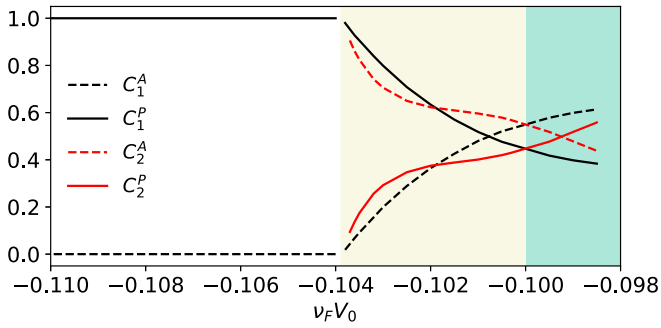

FIG. 3. The amplitude and phase character strengths C_m^A, C_m^P, respectively, for mode m in A_{1g} irreps. In the TRS side, the mode is pure phase one. In the TRS broken side, the characters mix and the phase-dominant mode 1 evolves into an amplitude-dominant one, whereas the amplitude-dominant mode 2 evolves into a phase-dominated one. All parameters are the same as in Fig. 2.

the spectral weights of the modes. In Fig. 2, we restricted ourselves to those B_{1g} interactions that are weak enough such that a transition to the $s + id$ state is preceded by that to the $s + is$ one.

In the remainder of this paper, we will analyze the above spectrum and its variations to potentially deduce the sign of gaps in the bands, their interplay with the Raman vertices, and the sign of interband interaction, wherever possible. We will also illustrate the use of the recently discovered interaction-induced selectivity of collective modes [21] to make sense of the calculated spectral weights in the various scenarios. This rule, as a reminder, broadly associates the character of the collective modes to the Raman vertices and infers the relative spectral weights of the modes in the gap and near the 2Δ threshold. For a pair of bands a, b, the rule suggests that a fluctuation in irrep r with the form factor $\delta\phi_r^a \pm s\delta\phi_r^b$ couples to the Raman vertex with the form $\gamma_r^a \pm s\gamma_r^b$, respectively, where $s \equiv -\mathrm{sgn}[\Delta_a \Delta_b V_r^{ab}]$. Further, the mode $\delta\phi_r^a + s\delta\phi_r^b$ will be the lower-energy mode and hence in the gap, and $\delta\phi_r^a - s\delta\phi_r^b$ will be the higher-energy mode, which could be over the 2Δ threshold and hence be damped.

A. eRS in the A_{1g} channel

In the A_{1g} irrep, due to the self-consistency condition, we get $s = -\mathrm{sgn}[\Delta_a \Delta_b V_{A_{1g}}^{ab}] = 1$. This means that the in-phase mode ($\delta\phi_r^a + \delta\phi_r^b$) should be the low-energy mode and couple to eRS as $\gamma_{A_{1g}}^a + \gamma_{A_{1g}}^b$. This is indeed what is expected of the BAG mode. Perhaps because this mode is renormalized up to the plasmon and hence not relevant in the low-energy sector, it was missed in the literature that this mode would couple to the eRS spectrum via the $\gamma_{A_{1g}}^a + \gamma_{A_{1g}}^b$ combination of Raman vertices. The rule also implies that the out-of-phase mode ($\delta\phi_{A_{1g}}^a - \delta\phi_{A_{1g}}^b$) should be the higher-energy mode and couple to eRS as $\gamma_{A_{1g}}^a - \gamma_{A_{1g}}^b$. This is indeed the well-known result for the two-band Leggett mode [16]. In fact, in our model, where bands b, c are identical, we can expect the

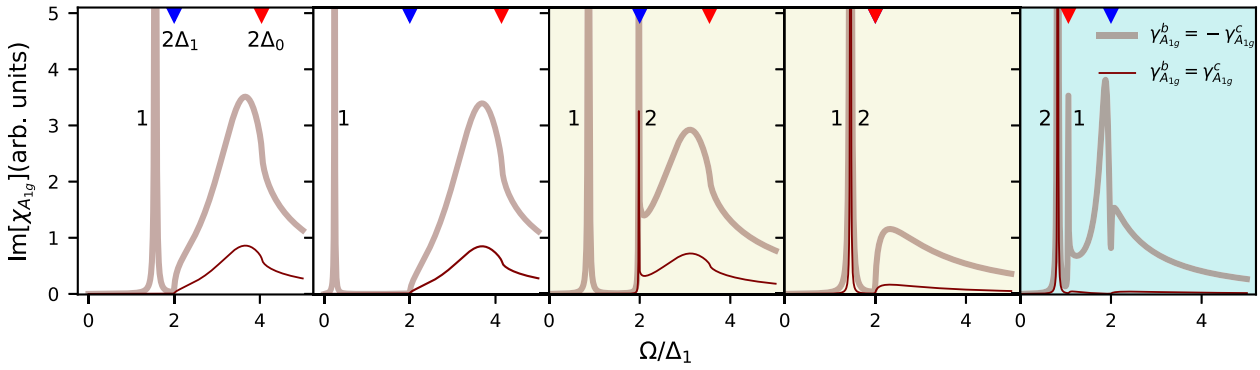

FIG. 4. A_{1g} response across the $s^{++} \to s + is$ transition for different choices of Raman vertices. The five panels are for $\nu_F V_0 \in \{-0.114, -0.104, -0.103, -0.1, -0.097\}$ from left to right. The background color corresponds to that shown in Fig. 1 with the white being the TRS phase, the yellow being the TRS broken phase, and the blue being deep in the TRS broken phase. The labels 1 and 2 track the long-lived collective modes shown in Fig. 2, and the two inverted triangles at the top track the evolution of the gaps Δ_1 (for bands b, c) and Δ_0 (for band a). All parameters are the same as in Fig. 2. Observe that mode 1 does not show up in eRS for $\gamma^b_{A_{1g}} = \gamma^c_{A_{1g}}$.

Leggett mode involving bands b, c not to couple (go dark) when $\gamma^b_{A_{1g}} = \gamma^c_{A_{1g}}$. This is exactly what we see in Fig. 4 on the TRS side, where we plot the eRS spectrum for select values of V_0. This serves as an example for a case where there could be a phase transition to the $s + is$ without any visible softening of a Leggett mode.

To better understand why the rules work the way they do, let us evaluate these general expressions explicitly on the TRS side by substituting for the Δ_α's and the Π^α_{ij}'s in Eq. (2). Using the expressions for l_α from the self-consistency relations, we get the response to be

$$\chi_{A_{1g}}(\Omega) = \left[\left(\gamma^a_{A_{1g}} - \gamma^b_{A_{1g}}\right)^2 + \left(\gamma^a_{A_{1g}} - \gamma^c_{A_{1g}}\right)^2\right]\frac{4\Delta_0\Delta_1/cV_0}{\Omega_1^2 - \Omega^2} + \left(\gamma^b_{A_{1g}} - \gamma^c_{A_{1g}}\right)^2 \frac{\left(4\Delta_1^2/V_1\right)\left(\Omega_3^2 - \Omega^2\right)}{\left(\Omega_1^2 - \Omega^2\right)\left(\Omega_2^2 - \Omega^2\right)}, \quad (13)$$

where

$$\Omega_1^2 = \left(\frac{1}{\nu_F^1 I_1} + \frac{2}{\nu_F^0 I_0}\right)\frac{2\Delta_0\Delta_1}{cV_0},$$

$$\Omega_2^2 = \frac{2\left(V_1\Delta_0\Delta_1 + 2cV_0\Delta_1^2\right)}{cV_0V_1\nu_F^1 I_1},$$

$$\Omega_3^2 = \frac{2\left(V_1\Delta_0^2 + 2V_0c\Delta_1\Delta_0\right)}{V_0^2\nu_F^0 I_0}.$$

Since the bands b, c are identical, we will have $|\gamma^b_{A_{1g}}| = |\gamma^c_{A_{1g}}|$. If all three effective mass vertices were identical, we would get a null response, which is expected, as we would recover the total charge vertex which does not fluctuate due to charge conservation. Here, we can note all the following relevant points: (i) All modes couple with $(\gamma_\alpha - \gamma_\beta)^2$ form factors, which explains why some modes can go dark if appropriate conditions on the vertices are met. (ii) We observe that the expression potentially hosts $n - 1 = 2$ poles (with $n = 3$). These are indicated by the frequencies Ω_1^2 and Ω_2^2 [56]. With only interband interactions, on the TRS side, we get one long-lived Leggett mode in the gap and the other mode beyond the 2Δ threshold. (iii) The self-consistency equations enforce $\mathrm{sgn}(cV_0) = -1$. This causes the result not to be sensitive to the phase of the ground state (s^{++} vs $s^{\pm}$), as c and V_0 always come as a product so that, when each switches sign, the result remains invariant.

Upon studying the character of the long-lived mode, we find that the fluctuating terms are indeed phaselike and such that phase terms from bands b, c are opposite in sign to each other without involving band a(see Appendix B). According to the rule such a mode should couple to effective Raman vertex $\gamma^b_{A_{1g}} - \gamma^c_{A_{1g}}$. This is why in Fig. 4 the Leggett mode only shows up for $\gamma^b_{A_{1g}} = -\gamma^c_{A_{1g}}$ and is dark for $\gamma^b_{A_{1g}} = \gamma^c_{A_{1g}}$.

In the TRS broken phase the general expressions become too unwieldy to show, but the A_{1g} response across the TRS breaking phase transition is plotted in Fig. 4 for two allowed cases of $\gamma^b_{A_{1g}} = \pm\gamma^c_{A_{1g}}$ for this model. The bounced-back mode (1) acquires an amplitude character with two characteristics (see Appendix B): it mixes amplitude and phase characters; and it mixes contributions from band a. What is interesting is that the contribution from band a only comes via the amplitude sector. The phase sector of the bounced-back mode is still exactly the same as it was on the TRS side. This is why the selectivity of the mode remains exact with respect to the choices of $\gamma^b_{A_{1g}} \pm \gamma^c_{A_{1g}}$ as is evident from the TRS broken panels of Fig. 4. While the fact that there is no phase component of band a is certainly an artifact of the model, this result, nevertheless, shows that the coupling of the collective modes to the eRS is entirely from the phase sector even in the TRS broken side. This is because if the phase sector of band a were to be involved, then the vertex combinations $\gamma^a_{A_{1g}} \pm \gamma^{b/c}_{A_{1g}}$ would contribute. Since band a is different from band b, c, the selection would not be exact. But we see in Fig. 4 an exact selectivity for the mode 1.

The second mode (2) that emerges from 2Δ region also has mixed character from all the bands, but importantly involves the phase fluctuations from band a (see Appendix B). According to the rule, we will now have contributions from $\gamma^a_{A_{1g}} \pm \gamma^{b/c}_{A_{1g}}$ vertices, and thus the spectral weight from this mode should be finite, but different, in the two choices of Raman vertices in Fig. 4. This is indeed what the plot shows.

We will see below that this feature that the phase part of the fluctuations of a mode is what couples to eRS, remains true in every case we analyze. Note also that the phase character of mode 2 with respect to bands b, c is the opposite of mode 1.

It is also evident from Fig. 4 that the entry into the TRS broken phase is not marked with any characteristic change at frequencies beyond the $2|\Delta|$ region, although deep inside the TRS broken state, the spectrum above $2|\Delta|$ acquires sharper features. We think that this is probably a feature of this model and nothing generic. Finally, even in the TRS broken phase, just like the TRS phase, we verified explicitly that changing the phase of the ground state on the TRS side from s^{++} to s^{+-} (by changing $V_0 \to -V_0$) did not alter the response.

B. Raman response in the B_{1g} channel

The advantage of eRS is that the same experiment provides access to not just excitations in the $r = A_{1g}$ irrep but also in other irreps. We can take a look at the $r = B_{1g}$ irrep to analyze how the spectrum could evolve across a TRS breaking transition. Studying this response requires no new calculations. The ground state remains the same as that in all the cases considered for $r = A_{1g}$. What is different here is that $V^{\rm pp}_{B_{1g},\alpha\beta}$ is now a parameter that is independent of the ground state and thus can be anything. This largely increases the phase space of possibilities. However, to lay within the scope of this paper, we can focus on the interband driven B_{1g} interactions modeled as

$$V^{\rm pp}_{B_{1g}} \to \begin{pmatrix} 0 & U_0 & U_0 \\ U_0 & 0 & U_1 \\ U_0 & U_1 & 0 \end{pmatrix}. \tag{14}$$

We can now explore the contribution of each of the interband interactions. Note that, in the limiting cases we will consider below by setting U_0 or U_1 to zero, the ground state always remains coupled with the phase diagram of Fig. 1.

The discussion of spectral weights of the resulting modes in the B_{1g} channel will involve many cases because $s = -\text{sgn}[\Delta_a \Delta_b V^{ab}_{B_{1g}}]$ can switch sign based on the phase of the ground state or the attractive or repulsive nature of the B_{1g} interaction (compared with the A_{1g} case, where $s = 1$). We shall discuss them on a case-by-case basis. For definiteness, our ground state will be of the s^{++} nature such that bands a and b, c are in phase on the TRS side. We will discuss the results for an s^{+-} state (opposite phase between bands a and b, c) whenever appropriate.

1. No B_{1g} interactions

In the limit $U_0, U_1 \to 0$, the response in the TRS and TRS broken phases is simply that of three independent bands, which is the addition of $1/\sqrt{\Omega - 2\Delta_0}$ and $1/\sqrt{\Omega - 2\Delta_1}$ features. We do not discuss this further. Further, if there are purely repulsive interactions such that there are no long-lived collective modes, we simply get some broad features near $2\Delta_1$ and $2\Delta_0$.

2. One decoupled band

Consider the limit $U_0 \to 0$ but with finite U_1. The fluctuations of the system are such that those from band a (order parameter Δ_0) are decoupled from the rest. In this case, we expect to get a noninteracting single-band response from band a leading to a $1/\sqrt{\Omega - 2\Delta_0}$ feature. This feature is evident all across the transition in both panels (for repulsive and attractive U_1) in Fig. 5. Since this feature belongs to band a, this part of the response is not sensitive to $\gamma^b_{B_{1g}} = \pm\gamma^c_{B_{1g}}$.

Added to this response will be that of a two (identical)-band scenario, where the fluctuations are coupled via interband interactions (U_1). For the bands b, c, which are always in phase in the TRS side, we get $s = -\text{sgn}[\Delta_b \Delta_c U_1] = -\text{sgn}[U_1]$. This means that the low-energy mode (within the gap) should have the form factor $\delta\phi^b_{B_{1g}} + s\delta\phi^c_{B_{1g}} = \delta\phi^b_{B_{1g}} - \text{sgn}[U_1]\delta\phi^c_{B_{1g}}$. This should couple to eRS as $\gamma^b_{B_{1g}} - \text{sgn}[U_1]\gamma^c_{B_{1g}}$. Thus, for a repulsive interband interaction ($U_1 > 0$), we expect the lower-energy BaSh mode to have an out-of-phase character, suggesting that, if it led to an $s + id$ ground state, it would be one with opposite phases in bands b and c. For an attractive U_1 interaction, the in-phase mode becomes the lower-energy mode. Further, the Raman vertex that picks up the spectral weight would also differ in each of these cases in accordance with the selection rule. All these points are exactly what we see in the two panels of Fig. 5. The characters of the modes in each case are also presented in Appendix B for verification.

Upon entering the TRS broken phase, many interesting observations can be made. Staying with mode 1 for $\gamma^b_{B_{1g}} = -\gamma^c_{B_{1g}}$, we see that the selectivity is still maintained despite the mixing from the amplitude sector (see Appendix B). This further supports that, even in the TRS broken phase, only the phase fluctuations couple to the eRS spectrum. Mode 1 also loses spectral weight to the $2\Delta_1$ peak deep inside the TRS broken state. This is understood also from the selection rule. For identical bands with pure interband interactions, there are two modes, one attractive and one repulsive, with the in-phase mode coupling to $\gamma^b_{B_{1g}} + \gamma^c_{B_{1g}}$ and the out-of-phase to $\gamma^b_{B_{1g}} - \gamma^c_{B_{1g}}$ [21]. Deep inside the TRS broken phase, where $\Delta_b \approx -\Delta_c$, there is a switch in $s = -\text{sgn}[\Delta_b \Delta_c U_1]$. This would switch the association of the spectral weights of the modes from one vertex to the other, manifesting in the transfer of spectral weight from the collective mode to the $2\Delta_1$ peak for the vertex $\gamma^b_{B_{1g}} = -\gamma^c_{B_{1g}}$. This is exactly what is seen in Fig. 5 in both panels. For the vertex $\gamma^b_{B_{1g}} = \gamma^c_{B_{1g}}$, the spectral weight moves to the collective mode.

Moving to mode 2, we observe that it is induced with a phase character opposite to that of mode 1 (see Appendix B). This aspect is true for both panels and means that mode 2 should be visible in the Raman vertex combination opposite to that of mode 1. This complimentary nature of modes 1 and 2 is clearly evident from both panels in Fig. 5.

It was pointed out in Ref. [21] that the response in the B_{1g} irrep is sensitive to the sign of the gaps in the ground state. While this is true in general, in this case, the s^{+-} phase in the TRS side would involve a sign change between bands a and b, c and not between b and c. Thus, with $U_0 = 0$ and the band a being decoupled from the rest, there would be no sensitivity to s^{++}/s^{+-} states. We explicitly verified that this is the case. Nevertheless, note that, deep in the TRS broken state, where $\Delta_b \approx -\Delta_c$, we did find the response to change

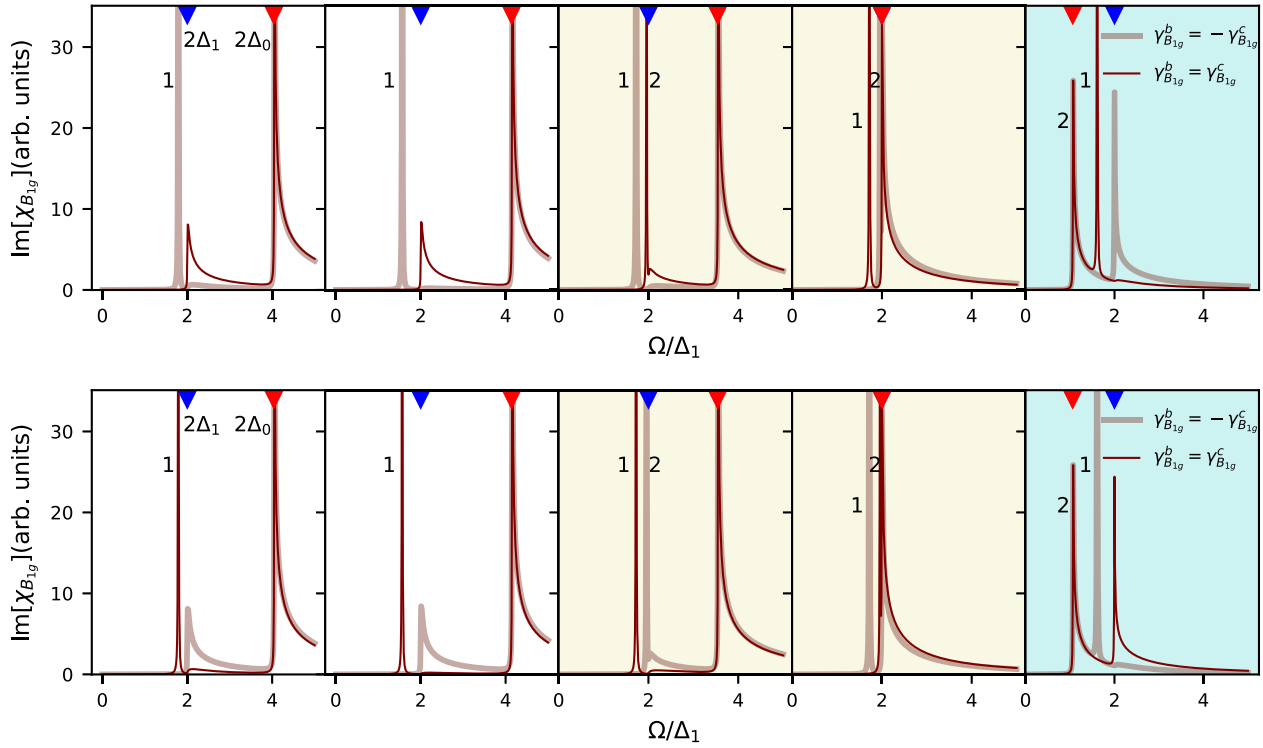

FIG. 5. B_{1g} response, for $U_0 = 0$ and $\nu_F U_1 = 0.09$ (top panel), $\nu_F U_1 = -0.09$ (bottom panel), across the $s^{++} \to s + is$ transition for different choices of Raman vertices. All panels follow the same convention as in Fig. 4 and are plotted for the same parameters. Observe that, in all cases, the spectral weights switch from the collective mode to the $2\Delta_1$ region or vice versa after the TRS breaking transition. Since fluctuations from band a are decoupled in this choice of interactions, the $2\Delta_0$ threshold peak always remains intact for different choices of Raman vertices and across the TRS breaking transition.

in a characteristic manner, in support of the above sensitivity claim.

3. *All coupled bands*

Consider the other limit of interband interactions was $U_1 \to 0$ but with finite U_0, where the fluctuations of all bands are coupled. In this case, since $U_1 = 0$, the two bands b, c effectively act as a unit. However, they do so in the following manner. Because they are simultaneously driven by band a, the effective interaction that would emerge between bands b and c is such that the intraband and interband interactions between these bands are the same (and repulsive). In such a system, the collective modes could be thought of as being derived from the interaction of band a with the subsystem b, c. In the subsystem b, c, one can form in-phase and out-of-phase modes, with coupling tendency to $\gamma^b_{B_{1g}} + \gamma^c_{B_{1g}}$ and $\gamma^b_{B_{1g}} - \gamma^c_{B_{1g}}$, respectively. The out-of-phase mode remains decoupled while the in-phase mode couples to the fluctuations of band a to give modes of the form $\delta\phi^a \pm \delta\phi^{b/c}$ which couple to eRS as $\gamma^a_{B_{1g}} \pm \gamma^{b/c}_{B_{1g}}$, respectively, where $\delta\phi^{b/c} \propto \delta\phi^b + \delta\phi^c$ and $\gamma^{b/c}_{B_{1g}} \propto \gamma^b_{B_{1g}} + \gamma^c_{B_{1g}}$. As per the selection rule, $s = -\mathrm{sgn}[\Delta_a \Delta_b U_0] = -\mathrm{sgn}[U_0]$. Then for the repulsive interaction, we can claim that the $\delta\phi^a - \delta\phi^{b/c}$ mode would be the lower-energy mode and the $\delta\phi^a + \delta\phi^{b/c}$ mode would be the higher-energy one. These two modes would be visible in both choices of the Raman vertices due to incomplete cancellations due to the presence of $\gamma^a_{B_{1g}}$. The relative phase mode from b, c, however, would couple as $\gamma^b_{B_{1g}} - \gamma^c_{B_{1g}}$ and hence be selective. This is indeed the observation in Fig. 6. It so happens that, in the chosen model, the $\delta\phi^b - \delta\phi^c$ mode is $\approx 2\Delta_1$. The characters of the modes that are presented in Appendix B confirm the above expectations.

Upon entering the TRS broken side, the BaSh mode 1 in the gap turns back. Despite mixing in of the amplitude character, its phase character remains the same. Just like in the previous subsection, there is also an additional collective mode 2 that emerges from the $2\Delta_1$ region. The character of this mode is such that amplitude fluctuations from all bands contribute, but the phase ones do so only from bands b, c, also in an out-of-phase manner (Appendix B). If only the phase sector of the mode is coupled to the eRS, then we should expect this part of the spectrum to only be visible for the vertex choice of $\gamma^b_{B_{1g}} - \gamma^c_{B_{1g}}$. This is indeed what is seen in Fig. 6.

Finally, we note that the above evolution was for the s^{++} state. If we change the ground state on the TRS side to s^{+-}, then from the selectivity rule, we expect that this should swap the evolution of $U_0 > 0$ with that of $U_0 < 0$. This swap is evident when Fig. 7 is compared with Fig. 6.

VI. CONCLUSIONS

We have extended the theory of eRS for a general multiband singlet superconductor to include the case of TRS breaking and traced the response in the different irreps. We

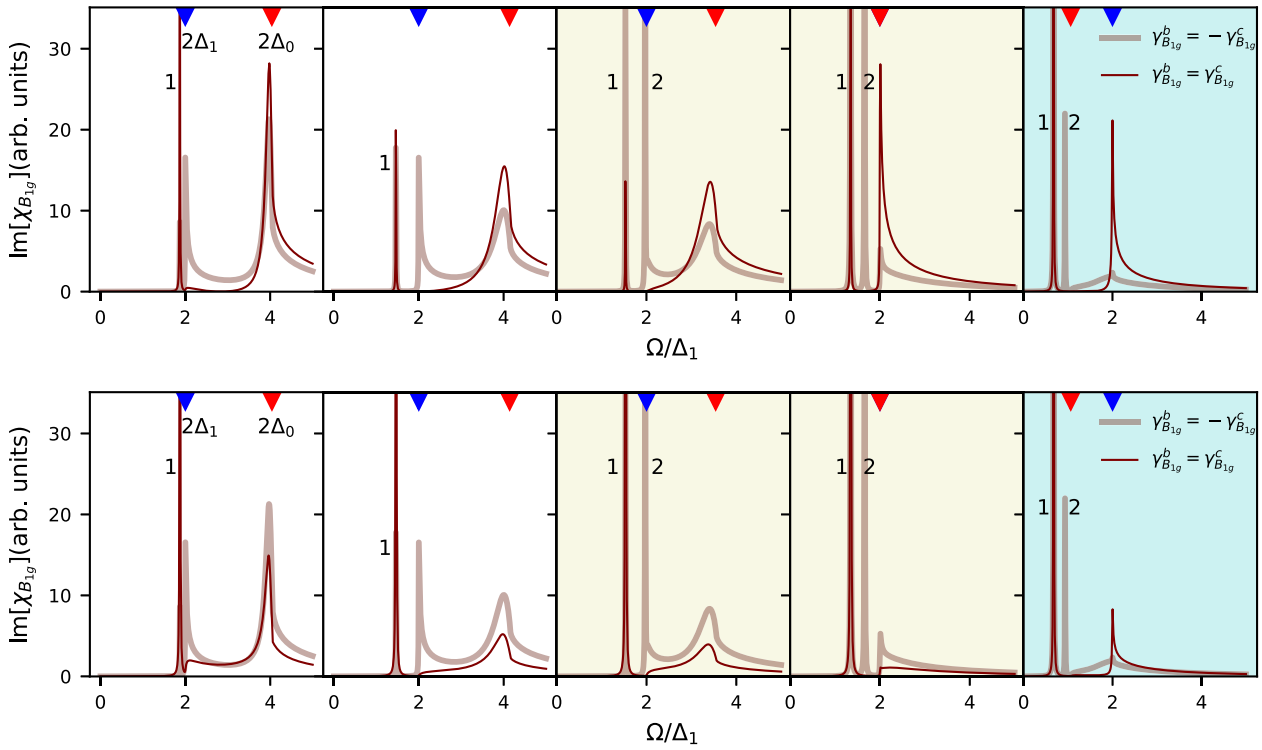

FIG. 6. B_{1g} response, for $U_1 = 0$ and $\nu_F U_0 = 0.07$ (top panel), $\nu_F U_0 = -0.07$ (bottom panel), across the $s^{++} \to s + is$ transition for different choices of Raman vertices. All other parameters are the same as in Fig. 5. Mode 1 includes phase character from band a and thus couples to the Raman vertex which contains $\gamma^a_{B_{1g}} \neq \pm\gamma^{b/c}_{B_{1g}}$. That is why it has finite spectral weight for both choices of Raman vertices. Mode 2 inside the TRS broken phase involves phase fluctuations only from bands b and c, and hence, the selectivity is exact, and this part of the spectrum is visible in only one choice of Raman vertex. The change in sign of U_0 does not affect the relative physics between band b, c, and hence, the selectivity remains.

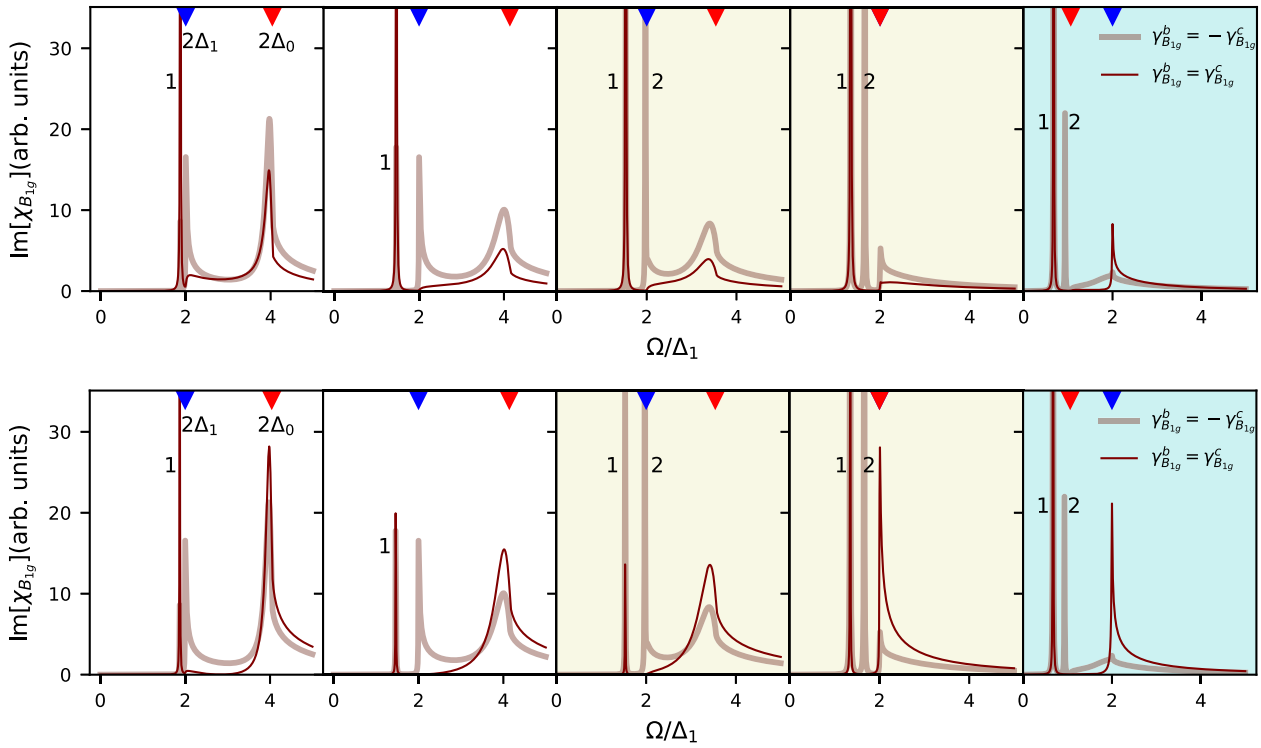

FIG. 7. B_{1g} response, for $U_1 = 0$ and $\nu_F U_0 = 0.07$ (top panel), $\nu_F U_0 = -0.07$ (bottom panel), across the $s^{+-} \to s + is$ transition for different choices of Raman vertices. All other parameters are the same as in Fig. 6. The only change from Fig. 6 is that the $U_0 > 0$ and $U_0 < 0$ panels are switched, which is to be expected, as the selection rule is sensitive to $\mathrm{sgn}[\Delta_a \Delta_{b/c} U_0]$.

also prescribed a way to characterize the fluctuation form factors, showing the equivalence between the Raman vertex and linear response kernel. We show that, even when the TRS is broken, where the collective modes are expected to have a mixed amplitude and phase character, the coupling to eRS is only through the phase sector of the mode.

We demonstrated the gauge invariance of the formalism in the TRS phase, reproduced the usual softening of the Leggett mode in A_{1g}, and showed that the TRS broken state is characterized by the introduction of another mode into the gap. While this mode has admixture from the amplitude sector, its phase character is opposite to the already existing Leggett mode. We also showed that there is a simultaneous tendency for a BaSh mode to soften in the B_{1g} response, driven by A_{1g} interactions and the proximity to the TRS broken state, a feature that has already been reported in the context of $Ba_{1-x}K_xFe_2As_2$ [13,57].

While our formalism naturally calculates the spectral weights of all the modes, we also demonstrated the consistency of these weights with the interaction-induced selection rule [21], pointing out certain cases where there could be dark Leggett and BaSh modes, thereby triggering a TRS breaking phase transition without a visible softening of the collective mode. We even identified features in the spectrum that arise due to the sign change of the order parameter in the TRS broken phase.

These results provide a comprehensive view of the low-energy collective modes in multiple symmetry channels within the linear response. Although the specific results discussed are for a three-band model, the formalism is applicable to any number of bands. Knowing this formalism and the response, one is now in a better position to model systems with the chiral $d+id$, $p+ip$ states, or even the nonlinear responses such as in the terahertz third-harmonic generation experiments. These would be some future goals for extending this formalism.

ACKNOWLEDGMENTS

We would like to acknowledge useful conversations with I. Benek-Lins. S.S. and S.M. were funded by the Natural Sciences and Engineering Research Council of Canada Grant No. RGPIN-2019-05486. S.S. was supported by the Horizon Postdoctoral Fellowship from Concordia University.

APPENDIX A: STRUCTURE OF $[\Pi^{\alpha}_{ij}]$

Consider explicitly $\mathrm{Det}[\Pi^{\alpha}_{ij}]$, with $\Pi^{\alpha}_{11} \to \chi^{\alpha}_{11} \equiv \Pi^{\alpha}_{11} + 2v_F l_\alpha$, and $\Pi^{\alpha}_{22} \to \chi^{\alpha}_{22} \equiv \Pi^{\alpha}_{22} + 2v_F l_\alpha$, where $i, j \in \{1,2,3\}$. This is given by

$$\begin{aligned}\mathrm{Det}\big[\Pi^{\alpha}_{ij}\big] &= \chi^{\alpha}_{11}\big(\chi^{\alpha}_{22}\Pi^{\alpha}_{33} - \Pi^{\alpha}_{32}\Pi^{\alpha}_{23}\big) - \Pi^{\alpha}_{12}\big(\Pi^{\alpha}_{21}\Pi^{\alpha}_{33} - \Pi^{\alpha}_{23}\Pi^{\alpha}_{31}\big) + \Pi^{\alpha}_{13}\big(\Pi^{\alpha}_{21}\Pi^{\alpha}_{32} - \chi^{\alpha}_{22}\Pi^{\alpha}_{31}\big)\\ &= \chi^{\alpha}_{11}\chi^{\alpha}_{22}\Pi^{\alpha}_{33} + \chi^{\alpha}_{11}\big(\Pi^{\alpha}_{23}\big)^2 + \big(\Pi^{\alpha}_{13}\big)^2\chi^{\alpha}_{22} - \big(\Pi^{\alpha}_{12}\big)^2\Pi^{\alpha}_{33} - 2\Pi^{\alpha}_{12}\Pi^{\alpha}_{23}\Pi^{\alpha}_{13}. \end{aligned} \tag{A1}$$

Plugging in the form of correlation functions Π^{α}_{ij} listed in Eq. (4), we get

$$\begin{aligned}\frac{\mathrm{Det}\big[\Pi^{\alpha}_{ij}\big]}{[\mathcal{I}_\alpha(\Omega)/|\Delta_\alpha|^2]^3} &= -\left[\frac{\Omega^2}{4} - \big(\Delta^R_\alpha\big)^2\right]\left[\frac{\Omega^2}{4} - \big(\Delta^I_\alpha\big)^2\right]\left[\big(\Delta^R_\alpha\big)^2 + \big(\Delta^I_\alpha\big)^2\right] - \left[\frac{\Omega^2}{4} - \big(\Delta^R_\alpha\big)^2\right]\frac{\Omega^2}{4}\big(\Delta^R_\alpha\big)^2\\ &\quad + \frac{\Omega^2}{4}\big(\Delta^I_\alpha\big)^2\left[\frac{\Omega^2}{4} - \big(\Delta^I_\alpha\big)^2\right] - \big(\Delta^R_\alpha\big)^2\big(\Delta^I_\alpha\big)^2\left[\big(\Delta^R_\alpha\big)^2 + \big(\Delta^I_\alpha\big)^2\right] + \frac{\Omega^2}{2}\big(\Delta^R_\alpha\big)^2\big(\Delta^I_\alpha\big)^2\\ &= 0. \end{aligned} \tag{A2}$$

This zero is essential to ensure the presence of the BAG mode in the charge neutral theory, thereby ensuring gauge invariance of the formalism.

APPENDIX B: BAND-RESOLVED CHARACTER OF THE MODES

We solve the eigenvalue problem of Sec. III B at the mode frequencies to find the eigenvector and from it deduce the weights of the amplitude and phase sectors. We show here the band-resolved amplitude and phase breakdown of the modes in each irrep to the left and right of the TRS breaking transition. The results have the structure χ^r_m, where for mode m in the rth irrep, the first three entries correspond to the amplitude, phase, and density components of band a, then the same for band b, and then the same

for band c. For the A_{1g} case, we have

$$\left[\chi_1^{A_{1g}}\right]_{v_F V_0=-0.104} = \begin{pmatrix} 0.00 \\ 0.00 \\ 0.00 \\ \hline 0.00 \\ 0.707 \\ 0.00 \\ \hline 0.00 \\ -0.707 \\ 0.00 \end{pmatrix}, \quad \left[\chi_1^{A_{1g}}\right]_{v_F V_0=-0.103} = \begin{pmatrix} -0.269 \\ 0.00 \\ 0.00 \\ \hline 0.252 \\ 0.632 \\ 0.00 \\ \hline 0.252 \\ -0.632 \\ 0.00 \end{pmatrix}, \quad \left[\chi_2^{A_{1g}}\right]_{v_F V_0=-0.103} = \begin{pmatrix} 0.00 \\ 0.54 \\ 0.00 \\ \hline -0.594 \\ 0.019 \\ 0.00 \\ \hline 0.594 \\ 0.019 \\ 0.00 \end{pmatrix}. \tag{B1}$$

We now show the band-resolved character for various choices of the B_{1g} interactions. For Fig. 5 and for $v_F U_1 = 0.09$, we get

$$\left[\chi_1^{B_{1g}}\right]_{v_F V_0=-0.104} = \begin{pmatrix} 0.00 \\ 0.00 \\ 0.00 \\ \hline 0.00 \\ 0.707 \\ 0.00 \\ \hline 0.00 \\ -0.707 \\ 0.00 \end{pmatrix}, \quad \left[\chi_1^{B_{1g}}\right]_{v_F V_0=-0.103} = \begin{pmatrix} 0.00 \\ 0.00 \\ 0.00 \\ \hline -0.387 \\ -0.591 \\ 0.00 \\ \hline -0.387 \\ 0.591 \\ 0.00 \end{pmatrix}, \quad \left[\chi_2^{B_{1g}}\right]_{v_F V_0=-0.103} = \begin{pmatrix} 0.00 \\ 0.00 \\ 0.00 \\ \hline 0.643 \\ -0.291 \\ 0.00 \\ \hline -0.643 \\ -0.291 \\ 0.00 \end{pmatrix}, \tag{B2}$$

For Fig. 5 and for $v_F U_1 = -0.09$, we get

$$\left[\chi_1^{B_{1g}}\right]_{v_F V_0=-0.104} = \begin{pmatrix} 0.00 \\ 0.00 \\ 0.00 \\ \hline 0.00 \\ 0.707 \\ 0.00 \\ \hline 0.00 \\ 0.707 \\ 0.00 \end{pmatrix}, \quad \left[\chi_1^{B_{1g}}\right]_{v_F V_0=-0.103} = \begin{pmatrix} 0.00 \\ 0.00 \\ 0.00 \\ \hline -0.387 \\ -0.591 \\ 0.00 \\ \hline 0.387 \\ -0.591 \\ 0.00 \end{pmatrix}, \quad \left[\chi_2^{B_{1g}}\right]_{v_F V_0=-0.103} = \begin{pmatrix} 0.00 \\ 0.00 \\ 0.00 \\ \hline 0.643 \\ -0.291 \\ 0.00 \\ \hline 0.643 \\ 0.291 \\ 0.00 \end{pmatrix}, \tag{B3}$$

For Fig. 6 and $v_F U_0 = 0.07$, we get

$$\left[\chi_1^{B_{1g}}\right]_{v_F V_0=-0.104} = \begin{pmatrix} 0.00 \\ 0.732 \\ 0.00 \\ \hline 0.00 \\ -0.481 \\ 0.00 \\ \hline 0.00 \\ -0.481 \\ 0.00 \end{pmatrix}, \quad \left[\chi_1^{B_{1g}}\right]_{v_F V_0=-0.103} = \begin{pmatrix} 0.00 \\ 0.723 \\ 0.00 \\ \hline 0.247 \\ 0.420 \\ 0.00 \\ \hline -0.247 \\ 0.420 \\ 0.00 \end{pmatrix}, \quad \left[\chi_2^{B_{1g}}\right]_{v_F V_0=-0.103} = \begin{pmatrix} 0.758 \\ 0.00 \\ 0.00 \\ \hline -0.397 \\ 0.233 \\ 0.00 \\ \hline -0.397 \\ -0.233 \\ 0.00 \end{pmatrix}, \tag{B4}$$

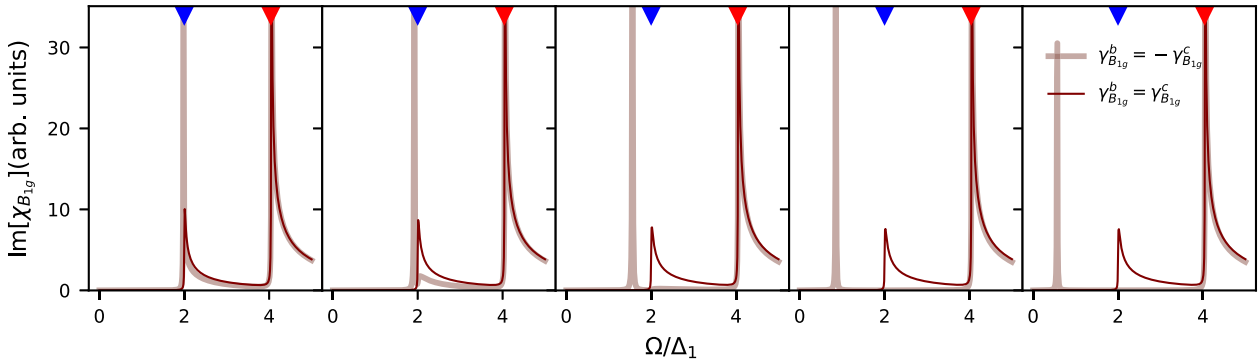

FIG. 8. B_{1g} response: BaSh mode softens as we increase the interaction U_1 in the d-wave channel. Here, we choose $U_0 = 0.00/v_F$, $V_0 = -0.114/v_F$, $v_F U_1 \in \{0.05, 0.075, 0.1, 0.11, 0.112\}$, and $\Delta_0/\Delta_1 = 2.02$.

For Fig. 6 and $v_F U_0 = -0.07$, we get

$$\left[\chi_1^{B_{1g}}\right]_{v_F V_0=-0.104} = \begin{pmatrix} 0.00 \\ 0.732 \\ 0.00 \\ \hline 0.00 \\ 0.481 \\ 0.00 \\ \hline 0.00 \\ 0.481 \\ 0.00 \end{pmatrix}, \quad \left[\chi_1^{B_{1g}}\right]_{v_F V_0=-0.103} = \begin{pmatrix} 0.00 \\ 0.723 \\ 0.00 \\ \hline -0.247 \\ -0.420 \\ 0.00 \\ \hline 0.247 \\ -0.420 \\ 0.00 \end{pmatrix}, \quad \left[\chi_2^{B_{1g}}\right]_{v_F V_0=-0.103} = \begin{pmatrix} 0.758 \\ 0.00 \\ 0.00 \\ \hline 0.397 \\ -0.233 \\ 0.00 \\ \hline 0.397 \\ 0.233 \\ 0.00 \end{pmatrix}. \tag{B5}$$

APPENDIX C: OTHER DEMONSTRATIVE EXAMPLES OF B_{1g} RESPONSE

Here, we just demonstrate a usual BaSh mode behavior for a multiband system with increasing strength of interband interaction. The BaSh mode softens as expected (see Fig. 8).

[1] R. Sooryakumar and M. V. Klein, Phys. Rev. Lett. **45**, 660 (1980).
[2] C. A. Balseiro and L. M. Falicov, Phys. Rev. Lett. **45**, 662 (1980).
[3] P. B. Littlewood and C. M. Varma, Phys. Rev. B **26**, 4883 (1982).
[4] M. V. Klein, Phys. Rev. B **25**, 7192 (1982).
[5] A. A. Abrikosov and L. A. Fal'kovski, P. Zh. Eksp. Teor. Fiz. **40**, 262 (1961) [Sov. Phys. JETP **13**, 179 (1961)].
[6] S. B. Dierker, M. V. Klein, G. W. Webb, and Z. Fisk, Phys. Rev. Lett. **50**, 853 (1983).
[7] R. Hackl, R. Kaiser, and S. Schicktanz, J. Phys. C **16**, 1729 (1983).
[8] T. P. Devereaux, D. Einzel, B. Stadlober, R. Hackl, D. H. Leach, and J. J. Neumeier, Phys. Rev. Lett. **72**, 396 (1994).
[9] T. P. Devereaux and D. Einzel, Phys. Rev. B **51**, 16336 (1995).
[10] T. P. Devereaux and R. Hackl, Rev. Mod. Phys. **79**, 175 (2007).
[11] G. Blumberg, A. Mialitsin, B. S. Dennis, M. V. Klein, N. D. Zhigadlo, and J. Karpinski, Phys. Rev. Lett. **99**, 227002 (2007).
[12] S. Maiti, T. A. Maier, T. Böhm, R. Hackl, and P. J. Hirschfeld, Phys. Rev. Lett. **117**, 257001 (2016).
[13] T. Böhm, F. Kretzschmar, A. Baum, M. Rehm, D. Jost, R. Hosseinian Ahangharnejhad, R. Thomale, C. Platt, T. A. Maier *et al.*, npj Quantum Mater. **3**, 48 (2018).
[14] V. K. Thorsmølle, M. Khodas, Z. P. Yin, C. Zhang, S. V. Carr, P. Dai, and G. Blumberg, Phys. Rev. B **93**, 054515 (2016).
[15] M. V. Klein, Phys. Rev. B **82**, 014507 (2010).
[16] T. Cea and L. Benfatto, Phys. Rev. B **94**, 064512 (2016).
[17] D. J. Scalapino and T. P. Devereaux, Phys. Rev. B **80**, 140512(R) (2009).
[18] A. V. Chubukov, I. Eremin, and M. M. Korshunov, Phys. Rev. B **79**, 220501(R) (2009).
[19] M. Khodas, A. V. Chubukov, and G. Blumberg, Phys. Rev. B **89**, 245134 (2014).
[20] S. Maiti, A. V. Chubukov, and P. J. Hirschfeld, Phys. Rev. B **96**, 014503 (2017).
[21] I. Benek-Lins and S. Maiti, Phys. Rev. B **109**, 104505 (2024).
[22] C. Nayak, S. H. Simon, A. Stern, M. Freedman, and S. Das Sarma, Rev. Mod. Phys. **80**, 1083 (2008).
[23] X.-L. Qi and S.-C. Zhang, Rev. Mod. Phys. **83**, 1057 (2011).
[24] G. M. Luke, A. Keren, L. P. Le, W. D. Wu, Y. J. Uemura, D. A. Bonn, L. Taillefer, and J. D. Garrett, Phys. Rev. Lett. **71**, 1466 (1993).

[25] E. R. Schemm, W. J. Gannon, C. M. Wishne, W. P. Halperin, and A. Kapitulnik, Science **345**, 190 (2014).
[26] G. M. Luke, Y. Fudamoto, K. M. Kojima, M. I. Larkin, J. Merrin, B. Nachumi, Y. J. Uemura, Y. Maeno, Z. Q. Mao, Y. Mori *et al.*, Nature (London) **394**, 558 (1998).
[27] J. Xia, Y. Maeno, P. T. Beyersdorf, M. M. Fejer, and A. Kapitulnik, Phys. Rev. Lett. **97**, 167002 (2006).
[28] E. R. Schemm, R. E. Baumbach, P. H. Tobash, F. Ronning, E. D. Bauer, and A. Kapitulnik, Phys. Rev. B **91**, 140506(R) (2015).
[29] V. Grinenko, P. Materne, R. Sarkar, H. Luetkens, K. Kihou, C. H. Lee, S. Akhmadaliev, D. V. Efremov, S.-L. Drechsler, and H.-H. Klauss, Phys. Rev. B **95**, 214511 (2017).
[30] V. Grinenko, R. Sarkar, K. Kihou, C. H. Lee, I. Morozov, S. Aswartham, B. Büchner, P. Chekhonin, W. Skrotzki, K. Nenkov *et al.*, Nat. Phys. **16**, 789 (2020).
[31] V. Grinenko, D. Weston, F. Caglieris, C. Wuttke, C. Hess, T. Gottschall, I. Maccari, D. Gorbunov, S. Zherlitsyn, J. Wosnitza *et al.*, Nat. Phys. **17**, 1254 (2021).
[32] R. Nandkishore, L. S. Levitov, and A. V. Chubukov, Nat. Phys. **8**, 158 (2012).
[33] C. Xu and L. Balents, Phys. Rev. Lett. **121**, 087001 (2018).
[34] C.-C. Liu, L.-D. Zhang, W.-Q. Chen, and F. Yang, Phys. Rev. Lett. **121**, 217001 (2018).
[35] S. Bhattacharyya, A. Kreisel, X. Kong, T. Berlijn, A. T. Rømer, B. M. Andersen, and P. J. Hirschfeld, Phys. Rev. B **107**, 144505 (2023).
[36] P. W. Anderson, Phys. Rev. **110**, 827 (1958).
[37] V. G. Vaks, V. M. Galitskii, and A. I. Larkin, P. Zh. Eksp. Teor. Fiz. **41**, 1655 (1962) [Sov. Phys.–JETP **14**, 1177 (1962)].
[38] I. Tüttö and A. Zawadowski, Phys. Rev. B **45**, 4842 (1992).
[39] S. Nakamura, Y. Iida, Y. Murotani, R. Matsunaga, H. Terai, and R. Shimano, Phys. Rev. Lett. **122**, 257001 (2019).
[40] P. W. Anderson, Phys. Rev. **112**, 1900 (1958).
[41] N. N. Bogoljubov, V. V. Tolmachov, and D. V. Širkov, Fortschr. Phys. **6**, 605 (1958).
[42] P. W. Anderson, Phys. Rev. **130**, 439 (1963).
[43] M. V. Klein and S. B. Dierker, Phys. Rev. B **29**, 4976 (1984).
[44] A. Bardasis and J. R. Schrieffer, Phys. Rev. **121**, 1050 (1961).
[45] A. J. Leggett, Prog. Theor. Phys. **36**, 901 (1966).
[46] A. A. Abrikosov and V. M. Genkin, P. Zh. Eksp. Teor. Fiz. **65**, 842 (1974) [Sov. Phys. JETP **38**, 417 (1974)].
[47] S.-Z. Lin and X. Hu, Phys. Rev. Lett. **108**, 177005 (2012).
[48] S. Maiti and A. V. Chubukov, Phys. Rev. B **87**, 144511 (2013).
[49] M. Marciani, L. Fanfarillo, C. Castellani, and L. Benfatto, Phys. Rev. B **88**, 214508 (2013).
[50] S. Maiti and P. J. Hirschfeld, Phys. Rev. B **92**, 094506 (2015).
[51] A. V. Balatsky, P. Kumar, and J. R. Schrieffer, Phys. Rev. Lett. **84**, 4445 (2000).
[52] W.-C. Lee, S.-C. Zhang, and C. Wu, Phys. Rev. Lett. **102**, 217002 (2009).
[53] N. R. Poniatowski, J. B. Curtis, A. Yacoby, and P. Narang, Commun Phys **5**, 44 (2022).
[54] S. Maiti and A. V. Chubukov, Phys. Rev. B **82**, 214515 (2010).
[55] This model, where the bands b, c were seen as pockets, was used in Ref. [48].
[56] These are transcendental equations in general which may or may not have solutions that correspond to long-lived modes.
[57] T. Böhm, A. F. Kemper, B. Moritz, F. Kretzschmar, B. Muschler, H.-M. Eiter, R. Hackl, T. P. Devereaux, D. J. Scalapino, and H.-H. Wen, Phys. Rev. X **4**, 041046 (2014).